Journal of Colloid and Interface Science 430 (2014) 200–206

Contents lists available at ScienceDirect

Journal of Colloid and Interface Science

www.elsevier.com/locate/jcis

The influence of annealing temperature on the interface and photovoltaic properties of CdS/CdSe quantum dots sensitized ZnO nanorods solar cells

Xiaofeng Qiu [a,1], Ling Chen [a,1], Haibo Gong [b], Min Zhu [a], Jun Han [a], Min Zi [a], Xiaopeng Yang [a], Changjian Ji [c,a], Bingqiang Cao [a,*]

[a] *Key Lab of Inorganic Functional Material in Universities of Shandong, School of Material Science and Engineering, University of Jinan, Jinan 250022, China*
[b] *Helmholtz-Zentrum Berlin für Materialien und Energie, Hahn-Meitner-Platz 1, 14109 Berlin, Germany*
[c] *Department of Physics, Qilu Normal University, Jinan 250200, China*

ARTICLE INFO

Article history:
Received 28 April 2014
Accepted 26 May 2014
Available online 6 June 2014

Keywords:
Nanowire
Core–shell
Annealing
Raman
Interface alloy
Solar cell

ABSTRACT

Arrays of ZnO/CdS/CdSe core/shell nanocables with different annealing temperatures have been investigated for CdS/CdSe quantum dots sensitized solar cells (QDSSCs). CdS/CdSe quantum dots were synthesized on the surface of ZnO nanorods that serve as the scaffold via a simple ion-exchange approach. The uniform microstructure was verified by scanning electron microscope and transmission electron microscope. UV–Visible absorption spectrum and Raman spectroscopy analysis indicated noticeable influence of annealing temperature on the interface structural and optical properties of the CdS/CdSe layers. Particularly, the relationship between annealing temperatures and photovoltaic performance of the corresponding QDSSCs was investigated employing photovoltaic conversion, quantum efficiency and electrochemical impedance spectra. It is demonstrated that higher cell efficiency can be obtained by optimizing the annealing temperature through extending the photoresponse range and improving QD layer crystal quality.

1. Introduction

Quantum dots-sensitized solar cells (QDSSCs) have attracted considerable attention due to their simple fabrication procedure and low cost [1–5]. Recently, intensive research efforts have been undertaken to develop QDSSCs with better performance. In particular, QDSSCs based on one-dimensional (1D) ZnO nanostructures, e.g., nanorods, nanowires and nanocables, grown on transparent conducting substrates have been reported [1,6–8]. With few grain boundaries, ZnO nanowires-based photoanodes can provide a direct pathway for rapid transport of photogenerated carriers to the collection electrodes [9]. In comparison to conventional mesoporous TiO_2 films, ZnO nanorods possess higher electron mobility, and its 1D nanostructure arrays can be grown easily on different substrates utilizing various methods [10–13]. On the other hand, various semiconductor QDs with narrow band gaps in the visible region, such as InAs, CdS, CdSe as well as ZnSe, have been adopted to sensitize 1D ZnO nanorods [14–17]. For instance, CdTe QDs were employed as sensitizers for QDSSCs, and the device performance was thoroughly discussed with particular attention on the control of the CdTe QDs sizes [18,19]. Furthermore, PbS QDs were also successfully synthesized on the ZnO nanowires (NWs), and the properties of the corresponding PbS sensitized solar cells were investigated [20,21]. Among all these semiconductor QDs sensitizers, CdS and CdSe QDs show more promising characteristics due to the light response in the visible region. Particularly, the formation of type-II core–shell heterogeneous nanocables with ZnO nanowires facilitates rapid separation and transportation of photon-generated carriers [3]. Wang et al. and Seol et al. [8,22] reported that ZnO nanowire arrays double-sensitized with CdS and CdSe QDs exhibited enlarged absorption range up to 650 nm and demonstrated improved photovoltaic performance. Nevertheless, it is obvious that the power conversion efficiencies of these QDSSCs are typically below the theoretically expected values (15–20%) [23]. How to prepare and optimize more efficient photoanodes should be a major challenge to further improve the cell efficiency. For example, many strategies have been adopted, like growing ZnO nanowires with large surface area to absorb more QDs [24,25], fabricating ZnO/TiO_2 hybrid electrodes [26], synthesizing MnTe-sensitized boron-doped TiO_2 and ZnO photoelectrodes

---

* Corresponding author. Fax: +86 531 8973 6292.
E-mail address: mse_caobq@ujn.edu.cn (B. Cao).

[1] These authors contributed equally.

http://dx.doi.org/10.1016/j.jcis.2014.05.057
0021-9797/© 2014 Elsevier Inc. All rights reserved.

[27], depositing a Al_2O_3 interface layer on the surface of the ZnO nanorods to retard carrier recombination between the semiconductor and liquid electrolyte [28,29]. As we know, although the ZnO nanowires are of single crystals, the subsequently synthesized QDs sensitizing layer has a typical polycrystalline structure. Improving their crystal quality is a necessary step to prevent the recombination of photo-generated carriers due to grain boundaries and interface defects. Annealing is a generally prerequisite post-growth step for the growth of polycrystalline film. It has been found that annealing at optimized temperature is necessary for solution-processed commercial CdTe/CdS polycrystalline thin film solar cells [30]. However, most of previous reports failed to illustrate the role of annealing treatment in sensitized photoanodes for QDSSCs in detail. Especially, the relationship between annealing condition and the interface structure and cell performance of the resulting QDSSC device was neglected.

In this paper, we aim at fabricating efficient photoanodes using well-aligned ZnO nanorods subsequently double-sensitized with CdS/CdSe QDs via optimizing the annealing temperature. A conformal and uniform CdS/CdSe coating was deposited on the surface of ZnO nanorod arrays by ion-exchange reaction to extend the absorption spectrum range effectively. Moreover, through modulation of annealing temperature, the relation between the photoanode crystalline microstructure and their corresponding solar cell performance was discussed.

2. Materials and methods

2.1. Growth procedure of ZnO nanorods

ZnO nanorods were grown through hydrothermal method on fluorine-doped tin oxide (FTO) glass substrates with aluminum-dope ZnO (AZO) seed layer. FTO glasses were cleaned with isopropanol, ethanol and acetone (volume ratio 1:1:1) by ultrasonication treatment. The cleaned FTO glass samples were further treated with UVO for 15 min to get rid of organic materials. For AZO seed layer, it was prepared on FTO glass by pulsed laser deposition (PLD) using AZO target which contains 2 wt% Al_2O_3 and 98 wt% ZnO. The deposition parameters are as follows: oxygen pressure 1.9 Pa, laser pulse with energy density of 200 mJ/cm^2, and frequency of 10 Hz, and substrate temperature of 25 °C. Then a solution composed of 25 mM zinc nitrate hydrate ($Zn(NO_3)_2{\cdot}6H_2O$) and 25 mM hexamethylenetetramine (HMTA) was prepared for growing ZnO nanorods. FTO glass substrate with AZO seed layer was immersed in the solution, where the FTO side was placed facedown. The beaker was kept at 95 °C for 12 h. The obtained ZnO nanorod film was rinsed with ethanol and deionized water several times. Finally, the film was annealed at 450 °C for 30 min to remove residual organic compounds.

2.2. Deposition of CdS and CdSe layers on the ZnO nanoarrays

The CdS/CdSe layer was deposited onto the ZnO nanorods by a simple ion-exchange process [7]. Briefly, ZnO nanorods were first immersed into a 100 mL solution containing 0.1 M $Na_2S{\cdot}9H_2O$ for 10 min at room temperature to form a thin ZnS layer, which serves as sacrificial template to convert into CdS via cation exchange. The sample was then immersed in the solution of 25 mM cadmium nitrate ($Cd(NO_3)_2$), 0.1 M thiourea (CN_2H_4S), and 0.1 M ethylenediamine ($C_2H_8N_2$) for 1 h at room temperature to get ZnO/CdS nanocable arrays. Subsequently, the ZnO/CdS nanocable arrays were immersed in a 30 mL Se^{2-} source solution (0.015 g of Se and 0.05 g of $NaBH_4$) and kept at 90 °C for 3 h to obtain the final ZnO/CdS/CdSe nanocable arrays. Finally, the samples were washed with deionized water and ethanol several times and then annealed in argon for 30 min at different temperatures.

2.3. Fabrication of CdS/CdSe sensitized ZnO nanorods solar cells

The prepared photoanodes with different annealing temperatures were assembled with Au counter electrodes and polysulfide electrolyte solution to fabricate sensitized solar cells. Then they were sealed by 25-μm thick polypropylene hot-melt films, and the interface of the cells was filled with a liquid electrolyte of 0.5 M Na_2S, 2.0 M sulfur, and 0.2 M KCl in water/methanol (3:7 in volume) solution. The active area of the solar cell was 0.6×0.6 cm^2 and the power conversion efficiency was measured immediately once the solar cell was sealed.

2.4. Materials and devices characterizations

X-ray diffraction (XRD, D8-Advance, Bruker) analysis was employed to characterize the crystalline properties of the AZO seed layer. The morphologies of the samples were observed by a Quanta FEG250 field emission scanning electron microscope (FE-SEM). Transmission electron microscope (TEM, JEM-2100F, JEOL) operated at 200 kV was utilized to analyze the microstructures of the samples. The element composition was measured with energy-dispersive X-ray spectrum (EDX, Inca, Oxford). The UV–Visible (UV–Vis) absorption spectrum was measured with a Shimadzu UV-3600 spectrophotometer. Raman spectral analyses were performed at room temperature with a Renishaw Raman microscope (inVia) excited with 514.5 nm laser. Photovoltaic measurements were recorded employing a 3A solar simulator (XES-40S1, San-Ei) with a simulated AM 1.5G illumination with a light intensity of 100 mW/cm^2. Current density–voltage (J–V) characteristics of the solar cells were measured with a Keithley 2612A source/meter. External quantum efficiency (EQE) of the devices was measured with QEX10 solar cell spectral response equipment (PV Measurement). The electrochemical impedance spectra (EIS) were carried out through electrochemical workstation (Zennium, ZAHNER) by applying open-circuit voltage under illumination of AM 1.5G 100 mW/cm^2 (10^{-1}–10^5 Hz) with a 10 mV AC signal.

3. Results and discussion

3.1. Microstructure and interface of ZnO/CdS/CdSe nanorods

The AZO seed layer was deposited on the FTO glass substrate by PLD in advance. Fig. 1(a) shows the surface morphology of such dense AZO layer composed of large pyramid-shaped nanoparticles, indicating the formation of polycrystalline film. From the XRD pattern in Fig. 1(b) we can find that, apart from several weak diffraction peaks at 26.6°, 37.9°, 51.6°, 61.7° and 65.6° due to the FTO substrate, three typical peaks at 31.8°, 34.4° and 36.3° can be ascribed to (110), (002) and (101) planes of the wurtzite ZnO, respectively. The intense peak at 34.4° with maximum intensity is far stronger than the others. It indicates that the prepared AZO seed layer exhibits a preferred orientation growth along c-axis. This is beneficial to the following ZnO nanorod array growth.

Fig. 2(a) shows a typical SEM image of ZnO nanorods grown on AZO-seeded FTO substrate. After the hydrothermal process, an array of ZnO nanorods about 2 μm in length is obtained, and the diameters are in the range of 50–200 nm. Smooth surfaces can be easily observed from the enlarged SEM image shown in Fig. 2(a). After depositing the CdS/CdSe shell via the ion-exchange approach, the ZnO/CdS/CdSe core–shell nanocables exhibit rougher surfaces in comparison with the naked ZnO nanorods as shown in Fig. 2(b). In addition, a layer of CdS/CdSe nanoparticles covered

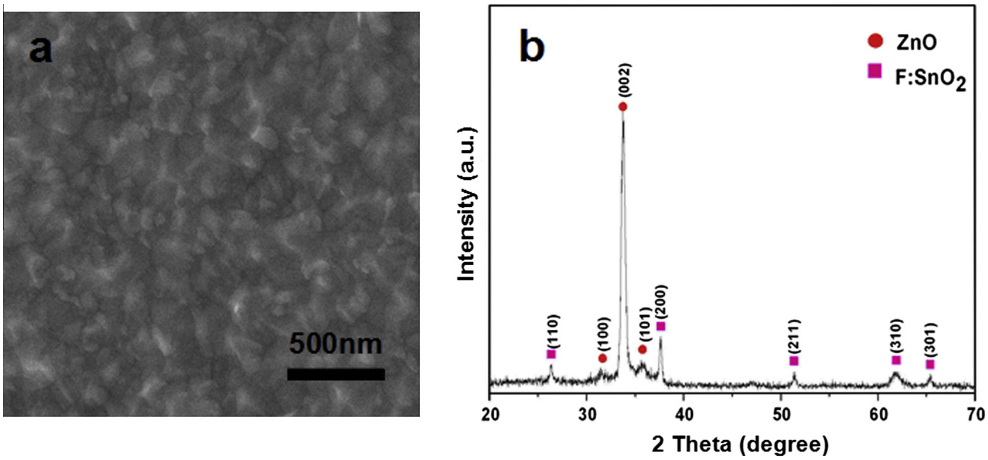

Fig. 1. (a) Top-view FESEM image and (b) XRD pattern of a typical AZO seed layer prepared by PLD on FTO glass substrate.

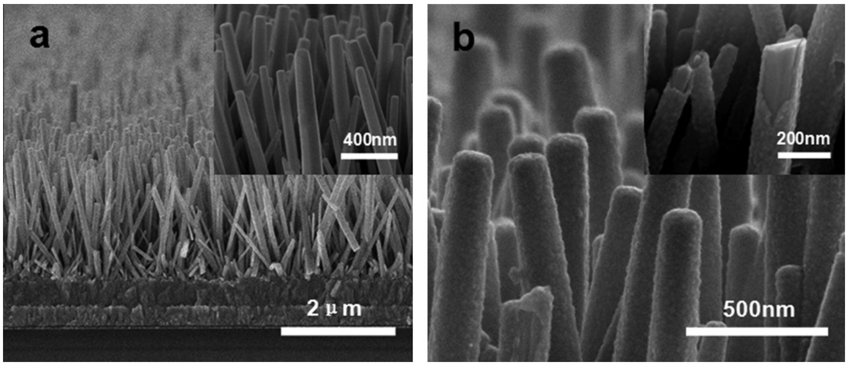

Fig. 2. (a) Cross-section and enlarged view SEM images of ZnO nanorod arrays grown for 12 h from a solution of $Zn(NO_3)_2$ and HMTA and (b) SEM images of ZnO/CdS/CdSe core–shell nanocables, for inset, a region where the shell has partially peeled off was deliberately chosen to show the formation of the core–shell structure.

conformally on the surface of ZnO nanorods, as depicted in the inset of Fig. 2(b) that was chosen to manifest the uniform coating of light-absorbing sensitizing layer. This will effectively prevent recombination between the photo-generated charge carriers and consequently, result in a significant improvement in QDSSCs efficiency due to the good coverage.

The microstructures of ZnO nanorod and ZnO/CdS/CdSe core–shell nanocable were further characterized with TEM. As shown in Fig. 3(a–c), the smooth surfaces of ZnO nanorod became rough after the growth of CdS shell and get rougher after partial exchanging Se^{2-} for S^{2-} in the outmost layer, which resulted from the formation of CdSe layer. Moreover, a high-resolution TEM image depicted in Fig. 3(d) demonstrated the typical core–shell structure grown on the surface of ZnO nanorod. HRTEM observation also revealed that the polycrystalline shell layer had an average thickness of ~20 nm and was composed of CdS QDs and CdSe QDs about 4~6 nm and 3~5 nm in diameter, respectively. The fringe spacings of the nanoparticles in the middle layer were measured to be ~0.34 nm and ~0.36 nm, which are consistent with the (002) and (100) planes of CdS. The fringe spacing of ~0.29 nm of the nanoparticles in the outer layer matches well with the interplanar spacing of the (101) plane of the cubic CdSe. In addition, the shell layer was further characterized by EDX mapping. Zn, Cd, S and Se elemental mappings are separately shown with different colors in Fig. 3(e–h), revealing homogeneous elements distribution through the shell. EDX analysis was further performed to calculate the component of the shell layer. A EDX spectrum (not shown here) indicates that the shell consists of cadmium and sulfur elements with an approximate atomic ratio of 1:1, which implies the formation of CdS shell. The corresponding EDX spectrum of ZnO/CdS/CdSe nanocable of Fig. 3(c) was shown in Fig. 3(i). S, Se and Cd components with an atomic ratio of nearly 5:12:18 were detected, which roughly suggested a CdSe/CdS molar ratio of 0.67/0.33. The simple was thus denoted as ZnO/$CdS_{0.33}Se_{0.67}$ in our work.

Raman spectroscopy was also employed for further analysis of crystallinity and interface of ZnO/CdS and ZnO/$CdS_{0.33}Se_{0.67}$ nanocable photoanodes annealed at various temperatures as illustrated in Fig. 4. For the ZnO/CdS photoanode (spectrum a), an intensive peak at 304.1 cm^{-1} is observed, which is the first-order longitudinal optical phonon mode (1LO) of CdS [31]. When the CdSe layer was deposited, the Raman peaks at about 300 nm still exist (spectra b–f), indicating only partial substitution of S^{2-} for Se^{2-} in the pre-formed CdS layer. At the same time, new Raman peaks are observed at around 200 cm^{-1} which belong to the typical 1LO mode of CdSe [32]. Moreover, after the formation of CdSe shell, new broad Raman bands appeared between the CdS-LO and CdSe-LO peaks, as shown in Fig. 4(b–e). These peaks are most probably attributed to the interface defects between CdS and CdSe layers formed during the ions exchange process [33] and the exact origin is still not very clear for us. It is interesting to note that when the ZnO/CdS/CdSe nanocable photoanode was annealed at 500 °C (Fig. 4e), the above interface defect-related peaks disappeared and the Raman spectrum exhibited typical double mode characteristics of $CdS_{1-x}Se_x$ semiconductor alloy [34]. That is a CdS-LO-like

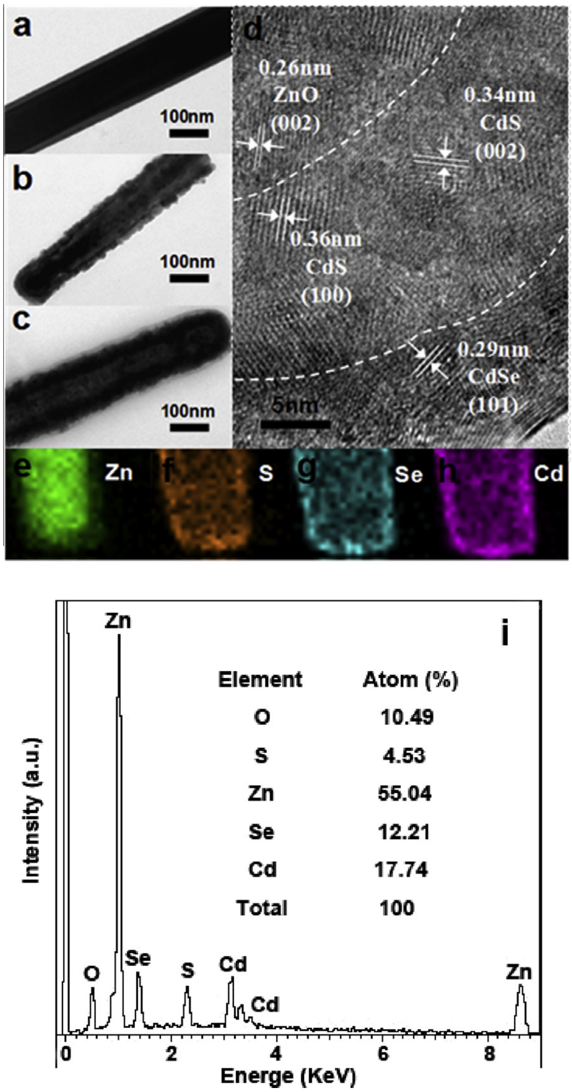

Fig. 3. TEM images of (a) a single ZnO nanorod; (b) ZnO/CdS and (c) ZnO/CdS/CdSe core–shell nanocables. (d) HRTEM image obtained from the surface region of a ZnO/CdS/CdSe core/shell nanocable and the corresponding EDX mappings of Zn, S, Se and Cd elements are illustrated in (e–h). Dashed lines are added for the interfaces between layers. (i) The EDX spectrum of ZnO/$CdS_{0.33}Se_{0.67}$ nanocable array corresponding to sample shown in (c).

peak at 290 cm^{-1} and a CdSe-LO-like peak at 213 cm^{-1} were both observed. But the LO peaks of CdS and CdSe were still observed although their intensity became weaker. This clearly indicates that the $CdS_{1-x}Se_x$ semiconductor alloy was formed at the CdS/CdSe shell interface after the annealing treatment. A more recent study by Tschirner et al. [33] found the $CdS_{1-x}Se_x$ alloy interface layer can be formed even without any annealing in the CdS@CdSe QDs by interdiffusion of selenium from the outermost layer into the CdS-layer. According to this double Raman LO-like peaks, we can estimate the $CdS_{1-x}Se_x$ composition approximately with $x = 0.7$ by an experiential formula calculation [34], which is well consisted with the EDX results. Last, it can be observed that when the CdS shell is partially changed to CdSe shell, the CdS-LO peak exhibits a clear downshift (spectrum b). This may be interpreted with the phonon confinement effect due to the decrease of CdS QDs size [35]. Then the CdSe-LO peak move back gradually (spectra c–e) and this can be explained by the smaller QDs growing up with increasing annealing temperature.

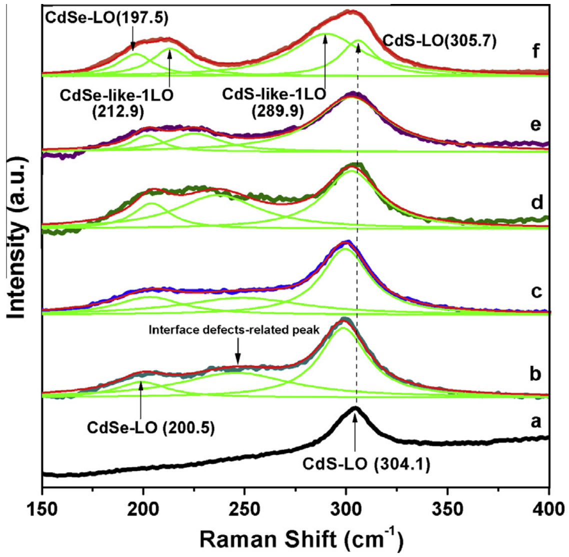

Fig. 4. Raman scattering spectra of the photoanodes with different annealing temperatures, under the excitation of 514.5 nm laser. Arrays of (a) ZnO/CdS nanocables annealed at 400 °C and ZnO/CdS/CdSe nanocables obtained at room temperature (b) and (e–f) annealed at 200 °C, 300 °C, 400 °C and 500 °C, respectively. The green lines are the Lorentz fitting results. (For interpretation of the references to color in this figure legend, the reader is referred to the web version of this article.)

3.2. Optical properties of ZnO/CdS and ZnO/$CdS_{0.33}Se_{0.67}$ core–shell nanocable arrays

Corresponding absorption spectra of the samples annealed at different temperatures are shown in Fig. 5. As-prepared ZnO nanorod shown in Fig. 5(a) exhibits an absorption edge at ~370 nm, matching well with the band gap (3.37 eV) absorption of ZnO nanorod. After depositing CdS shell on the surface of ZnO nanorod, the absorption edge of the ZnO/CdS nanocable (spectrum b) shifted to about 520 nm due to the smaller band gap of CdS (2.5 eV). Partially conversion of CdS to CdSe subsequently extended the optical absorption to the long wavelength direction. For as-prepared ZnO/CdS/CdSe nanocable (spectrum c), an absorption edge at about 600 nm was revealed. Interestingly, increasing the annealing temperature could further lead to a systematic shift of the absorption range to higher wavelength from 600 nm to 700 nm. Fig. 5 (spectra d–f) indicates that the light absorption range of ZnO/CdS/CdSe nanocable array could be effectively extended to almost the entire visible region by annealing temperature optimization. In detail, when annealed at 200 °C, the optical absorption of the nanocable remains unchanged. Such low-temperature could not cause any interface or size variation in double-sensitizing shell. As increasing the annealing temperature to 300 °C, subsequently to 400 °C, however, the absorption edge shifted to 650 nm and 700 nm, respectively. We attributed it to the increased QDs dimension due to their continuous growth as annealed at 300 °C and 400 °C. This result is consistent with the above Raman peak shifts in Fig. 4. The QDs show rather gradient absorption edge due to the diverse size distribution of CdS and CdSe QDs. Furthermore, the absorption edge of ZnO/CdS/CdSe nanocable annealed at 500 °C moves back to 640 nm. As both the CdS and CdSe LO peaks are weaker than the corresponding LO peaks from $CdS_{1-x}Se_x$ semiconductor alloy, we suppose the absorption is mainly from $CdS_{1-x}Se_x$ alloy and then a band gap about 1.94 eV is obtained. The band gap of $CdS_{1-x}Se_x$ alloy with a particular composition can be calculated with the following formula [36],

$$E_g(CdS_{1-x}Se_x) = xE_g(CdSe) + (1-x)E_g(CdS) + bx(1-x)$$

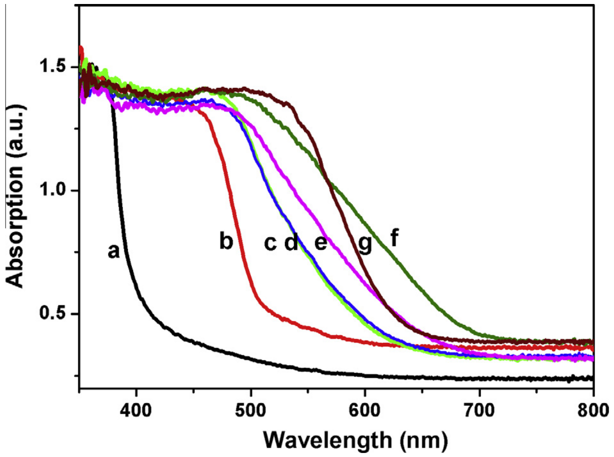

Fig. 5. UV–Vis absorption spectra of photoanodes annealed at different temperatures. Curves of (a) as-prepared ZnO nanorod; (b) ZnO/CdS nanocable annealed at 400 °C; (c) ZnO/CdS/CdSe nanocables obtained at room temperature, (d–g) nanocables annealed at 200 °C, 300 °C, 400 °C and 500 °C, respectively.

where E_g(CdSe) and E_g(CdS) are the band gaps of CdS and CdSe, respectively, and *b* is known as bowing parameter with reported value of 0.29 [37,38]. The $CdS_{1-x}Se_x$ band gap of 1.97 eV calculated by the above equation corresponds to $x \sim 0.7$, which agrees with the above result calculated by the Raman and EDX spectra.

3.3. Photovoltaic performance evaluation

Using the various ZnO/CdS/CdSe nanocable arrays annealed at different temperatures as the photoanodes, we fabricated QDSSCs to evaluate their photovoltaic (PV) performances. Fig. 6 (I) shows current density–voltage (*J–V*) curves of the cells. The corresponding device characteristics including short-circuit current density (J_{sc}), open-circuit voltage (V_{oc}), fill factor (FF), and power conversion efficiency (η) from various nanocables are summarized in Table 1. It is shown that the J_{sc} and η of ZnO/CdS/CdSe nanocable (curve b) are bigger than those of ZnO/CdS nanocable (curve a), which can be mainly explained by the extended absorption spectral response of the ZnO/CdS/CdSe nanocable with an additional CdSe layer as indicated by absorption spectra. Meanwhile, as increasing the annealing temperature, both the J_{sc} and η drastically increase to 3.12 mA/cm^2 and 0.39% for 200 °C (curve c), to 4.08 mA/cm^2 and 0.50% for 300 °C (curve d), and 4.80 mA/cm^2 and 0.72% for 400 °C (curve e) while their V_{oc} remains at about 0.40 V. It is worth mentioning that the $ZnO/CdS_{0.33}Se_{0.67}$ nanocable annealed at 500 °C reveals an improved V_{oc}, however, decreased J_{sc} as well as η.

Table 1
Photovoltaic parameters obtained by using the ZnO/CdS and $CdS_{0.33}/CdSe_{0.67}$ nanocable arrays as electrodes.

Sample	J_{sc} (mA/cm^2)	V_{oc} (V)	FF	η (%)
a	1.39	0.36	32.68	0.17
b	1.66	0.37	37.28	0.22
c	3.12	0.40	31.52	0.39
d	4.08	0.43	28.66	0.50
e	4.80	0.44	30.83	0.72
f	3.82	0.51	25.04	0.50

To further address the photoactivity of the photoanodes under different conditions quantitatively, the external quantum efficiency (EQE) of the solar cells was also measured, as presented in Fig. 6 (II). We can find the EQE of CdS/CdSe sensitized solar cell (curve b) is lower than that of CdS sensitized solar cell (curve a) in the range of 400–520 nm, although the J_{sc} and η were increased. The possible reason is that the defects in CdS/CdSe layer caused by the substitution of S^{2-} with Se^{2-} acting as recombination center leading to the destructive recombination between photo-generated carriers just before separation. When the ZnO/CdS/CdSe nanocable was annealed at 200 °C, EQE (curve c) of corresponding cell is generally larger than that of as-prepared (curve b) in the entire range of spectral response. Accordingly, the highly improved J_{sc} and η were observed. This may be attributed to the improved interface crystalline quality by annealing treatment with decreased recombination center. As the annealing temperature was further increased, for instance, from 300 °C to 400 °C, the J_{sc} and η were also improved due to the extended range of spectral response as shown in Fig. 6 (II, curve d–e). However, decreased J_{sc} and η were observed due to the narrowed spectral response range when the sample was annealed at 500 °C leading to interfacial alloying. Together with the corresponding absorption spectra in Fig. 5, we can see that the ZnO/CdS/CdSe nanocable array annealed at 400 °C has the best photovoltaic conversion.

3.4. Dynamic electrochemistry measurement

EIS was further carried out by applying bias of the open-circuit voltage in the dark over the frequency range of 10^{-1}–10^5 Hz to gain

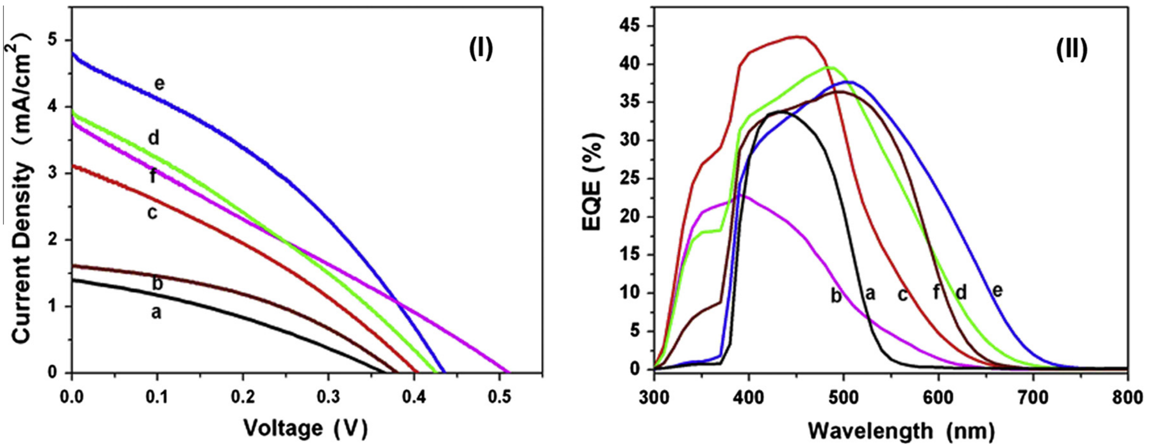

Fig. 6. (I) Current density–voltage (*J–V*) characteristics and (II) EQE spectra of the QDSSCs based on the (a) ZnO/CdS nanocable photoelectrode annealed at 400 °C and ZnO/CdS/CdSe nanocable photoelectrodes (b) obtained at room temperature, and (c–f) with different annealing temperatures which were annealed at 200 °C, 300 °C, 400 °C and 500 °C, respectively.

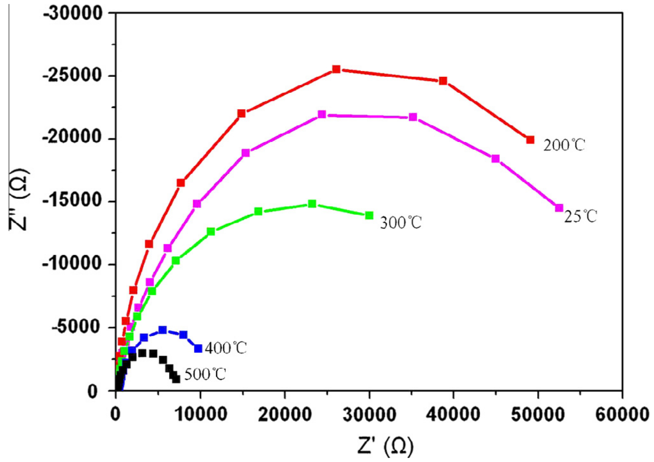

Fig. 7. Electrochemical impedance spectra (EIS) measurement of the ZnO/CdS/CdSe sensitized solar cells with different annealing temperatures.

the information on charge transport and recombination. Generally, from high to low frequency, the features successively represent electron diffusion in the mesoporous films (about 10 M to 10 K Hz), charge-transfer resistance at counter electrode (about 100 K to 1 K Hz), recombination resistance (about 1 K to 10 Hz) at mesoporous interface and redox couple shuttle diffusion (about 10 to 0.1 Hz) [39,40]. As shown in Fig. 7, the Nyquist plots of impedance express mainly as capacitive loops, which contain the frequency range of charge-transfer resistance at the interface of ZnO and $CdS_{0.33}/Se_{0.67}$ (denoted as R_s), as well as the recombination resistance between ZnO/$CdS_{0.33}/Se_{0.67}$ and electrolyte (denoted as R_{sh}). One can see from the capacitive loops that they differ in radiuses with different temperatures. Specially, when the temperature is higher than 200 °C, the radius drastically reduces. We accordingly speculate that increasing the annealing temperature can substantially change the electronic properties of the above two interfaces, that is, R_s and R_{sh}. Furthermore, any decrease in R_s and R_{sh} will lead to reduction of series resistance and shunt resistance of the QDSSCs, respectively. Reducing the former one theoretically benefits the performance of the cells, while decrease in the latter is against it due to serious leakage current between the ZnO/$CdS_{0.33}/Se_{0.67}$ and electrolyte interface [41,42]. As shown in Fig. 7, the major changes of capacitive loops occurred in the higher frequency range are mainly from charge-transfer resistance (R_s). Consequently, the decrease in radius of capacitive loop indicates decreased charge-transfer resistance existed in the interface between ZnO and $CdS_{0.33}/Se_{0.67}$. It is the result of interfacial crystalline quality improvement due to annealing. Smaller charge-transfer resistance means faster separation and reduced recombination between photo-generated carriers with a result of increased V_{oc}, as shown in Table 1.

4. Conclusion

In this paper, the conformal and uniform CdS and $CdS_{0.33}Se_{0.67}$ shells were synthesized on the ZnO nanorod arrays by simple ion-exchange method. And the influence of annealing temperatures on the microstructures and photovoltaic properties for ZnO/CdS/CdSe QDSSCs was investigated. The uniform core–shell microstructure of ZnO/CdS/CdSe nanorods was verified with SEM and TEM measurements. The absorption edge of ZnO/CdS/CdSe nanocable can be effectively extended to about 700 nm by annealing at 400 °C. Annealing at higher temperature than 400 °C results in a $CdS_{1-x}Se_x$ interface alloy layer formation between CdS and CdSe shells. A detailed analysis of the Raman spectra confirms the formation and composition of the $CdS_{0.33}Se_{0.67}$ alloy interface layer. A series of QDSSCs assembled with ZnO/CdS/CdSe nanocables annealed at different temperatures proved that their photovoltaic properties can be improved by extending the photoresponse range and enhancing the CdS/CdSe QDs layer crystal quality. More efforts like modifying the ZnO nanorods length or QDs layer thickness and finding solid hole transport materials are currently underway to further improve the photovoltaic efficiency.

Acknowledgments

This work is supported by NSFC (11174112) and Shandong Provincial Science Foundation for Disguised Youth Scholars (JQ201214). The research programs from Ministry of Education, China, are also acknowledged (NCET-11-1027, 213021A). BC thanks the Taishan Scholar Professorship (TSHW20091007) tenured at University of Jinan. A Project of Shandong Province Higher Educational Science and Technology Program (J11LA58) is also acknowledged.

References

[1] A. Kongkanand, K. Tvrdy, K. Takechi, M. Kun, P.V. Kamat, J. Am. Chem. Soc. 130 (2008) 4007–4015.
[2] J. Xu, C.Y. Luan, Y.B. Tang, X. Chen, J.A. Zapien, W.J. Zhang, H.L. Kwong, X.M. Meng, S.T. Lee, C.S. Lee, ACS Nano 4 (2010) 6064–6070.
[3] J. Xu, X. Yang, H.K. Wang, X. Chen, C.Y. Luan, Z.X. Xu, Z.Z. Lu, V.A.L. Roy, W.J. Zhang, C.S. Lee, Nano Lett. 11 (2011) 4138–4143.
[4] J. Chen, J. Wu, W. Lei, J.L. Song, W.Q. Deng, X.W. Sun, Appl. Surf. Sci. 256 (2010) 7438–7441.
[5] M. Graetzel, Nature 414 (2001) 338–344.
[6] Z.Z. Lu, J. Xu, X. Xie, H.K. Wang, C.D. Wang, S.Y. Kwok, T.L. Wong, H.L. Kwong, I. Bello, C.S. Lee, S.T. Lee, W.J. Zhang, J. Phys. Chem. C 116 (2012) 2656–2661.
[7] L. Chen, H.B. Gong, X.P. Zheng, M. Zhu, J. Zhang, S.K. Yang, B.Q. Cao, Mater. Res. Bull. 48 (2013) 4261–4266.
[8] X.N. Wang, H.J. Zhu, Y.M. Xu, H. Wang, Y. Tao, S.K. Hark, X.D. Xiao, Q. Li, ACS Nano 4 (2010) 3302–3308.
[9] K.S. Leschkies, R. Divakar, J. Basu, E. Enache-Pommer, J.E. Boercker, C.B. Carter, U.R. Kortshagen, D.J. Norris, E.S. Aydil, Nano Lett. 7 (2007) 1793–1798.
[10] J.J. Qiu, X.M. Li, F.W. Zhuge, X.Y. Gan, X.D. Gao, W.Z. He, S.J. Park, H.K. Kim, Y.H. Hwang, Nanotechnology 21 (2010) 195602.
[11] W.B. Wu, G.D. Hu, S.G. Cui, Y. Zhou, H.T. Wu, Cryst. Growth Des. 8 (2008) 4014–4020.
[12] B.J. Kwon, K.M. Lee, H.Y. Shin, J.w. Kim, J.Z. Liu, S. Yoon, S. Lee, Y.H. Ahn, J.Y. Park, Mater. Sci. Eng. B 177 (2012) 132–139.
[13] L.Y. Chen, Y.T. Yin, C.H. Chen, J.W. Chiou, J. Phys. Chem. C 115 (2011) 20913–20919.
[14] P. Yu, K. Zhu, A.G. Norman, S. Ferrere, A.J. Frank, A.J. Nozik, J. Phys. Chem. B 110 (2006) 25451–25454.
[15] Y. Tak, S.J. Hong, J.S. Lee, K.J. Yong, J. Mater. Chem. 19 (2009) 5945–5951.
[16] I. Robel, V. Subramanian, M. Kuno, P.V. Kamat, J. Am. Chem. Soc. 128 (2006) 2385–2393.
[17] K.S. Leschkies, R. Divakar, J. Basu, E. Enache-Pommer, J.E. Boercker, B.C. Carter, U.R. Kortshagen, D.J. Norris, E.S. Aydil, Nano Lett. 7 (2007) 1793–1798.
[18] P. Lekha, Avinash Balakrishnan, K.R.V. Subramanian, Shantikumar V. Nair, Mater. Chem. Phys. 141 (2013) 216–222.
[19] L. Chen, H.B. Gong, H.M. Wei, X. L Hu, H.Y. Xu, P. Liu, B.Q. Cao, Sci. Adv. Mater. 4 (2012) 337–341.
[20] H. Lee, H.C. Leventis, S.J. Moon, P. Chen, S. Ito, S.A. Haque, T. Torres, F. Nueesch, T. Geiger, S.M. Zakeeruddin, M. Graetzel, M.K. Nazeeruddin, Adv. Funct. Mater. 19 (2009) 2735–2742.
[21] H.B. Wang, T. Kubo, J. Nakazaki, T. Kinoshita, H. Segawa, J. Phys. Chem. Lett. 4 (2013) 2455–2460.
[22] M.S. Seol, H.J. Kim, Y.J. Tak, K.J. Yong, Chem. Commun. 46 (2010) 5521–5523.
[23] S. Rühle, M. Shalom, A. Zaban, Chem. PhysChem. 11 (2010) 2290–2304.
[24] C.K. Xu, J.M. Wu, U.V. Desai, D. Gao, J. Am. Chem. Soc. 133 (2011) 8122–8125.
[25] G. Jimenez-Cadena, E. Comini, M. Ferroni, A. Vomiero, G. Sberveglieri, Mater. Chem. Phys. 124 (2010) 694–698.
[26] B.S. Shaheen, H.G. Salem, M.A. El-Sayed, K.A. Nageh, J. Phys. Chem. C 117 (2013) 18502–18509.
[27] A. Tubtimtae, K. Arthayakul, B. Teekwang, K. Hongsith, S. Choopun, J. Colloid Interface Sci. 405 (2013) 78–84.
[28] S.K. Kim, M.K. Son, S.Y. Park, M.S. Jeong, K. Prabakar, H.J. Kim, Mater. Chem. Phys. 143 (2014) 1404–1409.
[29] J.P. Deng, M.Q. Wang, X.H. Song, Y.H. Shi, X.Y. Zhang, J. Colloid Interface Sci. 388 (2012) 118–122.
[30] Chul S. Kim, Ho B. Im, J. Am. Ceram. Soc. 73 (1990) 53–150.
[31] T. Thongtem, A. Phuruangrat, S. Thongtem, Ceram. Int. 35 (2009) 2817–2822.
[32] F. Comas, N. Studarta, G.E. Marquesa, Solid State Commun. 130 (2004) 477–480.

[33] N. Tschirner, H. Lange, A. Schliwa, A. Biermann, C. Thomsen, K. Lambert, R. Gomes, Z. Hens, Chem. Mater. 24 (2012) 311–318.
[34] A. Tu, P.D. Persans, Appl. Phys. Lett. 58 (1991) 1506–1508.
[35] A.V. Gomonnai, Y.M. Azhniuk, V.O. Yukhymchuk, M. Kranjčec, V.V. Lopushansky, Phys. Status. Solidi. B 239 (2003) 490–499.
[36] P.P. Ingole, G.B. Markad, D. Saraf, L. Tatikondewar, O. Nene, A. Kshirsagar, S.K. Haram, J. Phys. Chem. C 117 (2013) 7376–7383.
.[37] L.A. Swafford, L.A. Weigand, M.J. Bowers, J.R. McBride, J.L. Rapaport, T.L. Watt, S.K. Dixit, L.C. Feldman, S.J. Rosenthal, J. Am. Chem. Soc. 128 (2006) 12299–12306.
[38] S.H. Wei, S.B. Zhang, A.J. Zunger, J. Appl. Phys. 87 (2000) 1304–13011.
[39] F. Garcia-Belmonte, G. Mora-Sero, I. Bisquert, J. Phys. Chem. Chem. Phys. 13 (2011) 9083–9118.
[40] K.Y. Yan, Y.C. Qiu, W. Chen, M. Zhang, S.H. Yang, Energy Environ. Sci. 4 (2011) 2168–2176.
[41] K.Y. Yan, L.X. Zhang, J.H. Qiu, Y.C. Qiu, Z.L. Zhu, J.N. Wang, S.H. Yang, J. Am. Chem. Soc. 135 (2013) 9531–9539.
[42] G.Y. Lan, Z. Yang, H.T. Chang, J. Mater. Chem. 19 (2009) 2349–2355.